ELSEVIER

Atmospheric Research 69 (2003) 109–124

ATMOSPHERIC RESEARCH

www.elsevier.com/locate/atmos

Contribution of different scales to integral moisture transport based on aircraft observations over the Sea of Japan☆

M.Yu. Mezrin[a,*], E.V. Starokoltsev[a], Y. Fujiyoshi[b], M. Yoshizaki[c]

[a] *Central Aerological Observatory, 3 Pervomayskaya St., Dolgoprudny, Moscow Region, 141700, Russia*
[b] *Institute of Low Temperature Sciences, Hokkaido University, Japan*
[c] *Meteorological Research Institute, Japan Meteorological Agency, Japan*

Received 11 November 2002; accepted 6 April 2003

Abstract

Based on the Joint Research Agreement between the Central Aerological Observatory of the Russian Federal Service for Hydrometeorology and Environmental Monitoring (CAO), and the Core Research for Evolutional Science and Technology (CREST) of Japan Science and Technology Corporation (JST), a Russian research aircraft, IL-18, was employed to carry out investigations of the structure and formation/development mechanisms of mesoscale convective systems over the Sea of Japan area in January–February 2001.

Vertical moisture transport was one of the subjects of the experiment. To study it, the instruments installed on board the aircraft measured the oscillations of the vertical wind component w' and absolute air humidity ρ'. The vertical moisture transport was analyzed by an eddy correlation method using the formula $Q = \overline{w'\rho'}$. The technique was modified to determine the transport in a wider scale range, from 10 m to 50 km (0.1–500 s).

In the course of the experiment, an inflow of cold dry air from the continent (the Siberian area) was observed. As the air mass was moving towards Japan, it was getting warmer and more humidified due to heat and moisture exchange with the open surface of the Sea of Japan. The cloud streets formed testify to the presence of roll circulation. The mean integral moisture transport has proved to be about 0.07 g/m^2 s. Spectral analysis has revealed the following three scales by their input to moisture transport: 10–1000 m (turbulence), 1000–3000 m (convective cell), 3–10 km (convective body). Larger scales do not make any considerable input. At a 100-m altitude, the

☆ Discussed will be the integral (including different scales), mean (averaged over a horizontal path), and vertical moisture transport.

* Corresponding author. Tel.: +7-095-408-66-77; fax: +7-095-576-33-27.
E-mail address: mezrin@online.ru (M.Y. Mezrin).

doi:10.1016/S0169-8095(03)00041-3

contributions of all the three scales under consideration are equal, while at 500 m, the role of the largest one becomes more prominent. The share of turbulent flux is 1/3 and 1/6 at 100 and 500 m, respectively.

In the space structure of moisture transport obtained for altitudes of 100 and 500 m, 25-km features were detected, which were associated with the position of cloud streets that had formed at an altitude of 1000–1500 m. These features can be accounted for by roll circulation (horizontal roll vortices, organized roll vortices). A comparison of heat and moisture transports (in terms of sensible and latent heat fluxes) has indicated that their ratio at a 100-m altitude is close to 2, and at 500 m to 1. The difference between the values of the transport at the two altitudes agrees with the estimates of horizontal heat and moisture advection.

Keywords: Research aircraft; Boundary layer; Roll vortices; Flux; Scales

1. Introduction

Based on the Joint Research Agreement between the Central Aerological Observatory of the Russian Federal Service for Hydrometeorology and Environmental Monitoring (CAO), and the Core Research for Evolutional Science and Technology (CREST) of Japan Science and Technology Corporation (JST), a Russian research aircraft, IL-18, was employed to carry out investigations over the Sea of Japan area in January–February 2001.

The research flights were to clarify the dynamic and thermodynamic structure of mesoscale disturbances that develop over the Sea of Japan and their atmospheric environment.[1]

Vertical moisture transport was one of the subjects of the experiment. To investigate this matter, the instruments installed on board the aircraft measured the oscillations of the vertical wind component w' (Strunin, 1997) and absolute air humidity ρ' (Mezrin, 1997). The moisture transport was analyzed after the flight by an eddy correlation method using the formula $Q_w = \overline{w'\rho'}$. The technique to measure w' was modified to determine the transport in a wider scale range. The sensibility of the hygrometer measuring absolute air humidity (Ultraviolet Hygrometer, UVH) was continuously controlled by precision Aircraft Condensation Hygrometer, ACH (Mezrin and Starokoltsev, 2001).

[1] The processes of the atmosphere–ocean interaction in the Sea of Japan area are largely responsible for the weather and climate of Japan. Thus, a winter surge of cold, dry air from Siberia to the open sea surface leads to severe snowfalls in Japan. The intensive heat and moisture transport due to the large gradients of temperature and moisture content leads to fast development of the boundary layer as the air mass is nearing the coast of Japan (Murakami et al., 1994). Cloud streets are formed over the sea. A lot of observational and theoretical studies are devoted to this phenomenon (Fujiyoshi et al., 1998; Yoshimoto et al., 2000). Due to the lack and difficulty of direct observation in the Sea of Japan, it was hard to determine latent and sensible heat fluxes. These quantities were so far estimated based on routine upper-air sounding data (Kato and Asai, 1983).

2. Equipment and technique

In addition to air navigational equipment and instrumentation to measure moisture and heat transport, the airplane was fitted with some meteorological and geophysical instruments enabling the assessment of meteorological features accompanying the phenomenon being observed.

2.1. Measuring vertical wind speed component

$\Delta\alpha$ (°)—*Angle of attack* characterizing wind direction relative to the airplane. It is measured with a spherical five-hole pressure probe.

θ (°)—*Pitch angle—the angle between the airplane axis and horizontal.* Pitch angle variations are measured by gyros.

U (m/s)—*Airplane's true air speed* calculated by dynamic and static pressure, with the temperature of the outside thermometer taken into account.

Δn (g)—*Airplane's vertical acceleration* measured by gyrostabilized accelerometer.

Vertical wind speed variation, w, is calculated by the formula

$$w = (\Delta\alpha - \Delta\theta)U + W_p,$$

where $W_p = g\int_0^t \Delta n d\zeta$ is the aircraft vertical speed, g is the gravity constant.

As the formula includes several measured variables, the accuracy of calculating w was verified by analyzing a special flight mode comprising moderate wave-like aircraft motions ("steep climbs"), with all w components undergoing considerable changes. The resulting value was to remain undisturbed.

The instrumentation and technique described[2] enables measurements of the vertical component of wind speed within a range of 8–0.06 Hz. The low-frequency limitation is mainly due to the inaccuracy of data from vertical accelerometer, which are necessary for deriving aircraft vertical speed, W_p, by g-load integration.

In processing the data of the last experiment, the authors attempted to extend the range of measured oscillations of the vertical wind speed component to larger scales, while data on the vertical aircraft speed were obtained by differentiating the aircraft barometric height, i.e., the height derived from static pressure. Data analysis shows that the barometric height derivative H'_{bar} and g-load integral W_p closely correlate at time scales of 1–10 s and thus can be joined in this range.

$$w = (\Delta\alpha - \Delta\theta)U + (W_p)' + \overline{H'_{bar}}$$

$\overline{H'_{bar}}$ is derived by averaging barometric speed H'_{bar} by a 5-s sliding mean, $(W_p)'$ is derived by subtracting a 5-s sliding mean from W_p.

[2] Developed at CAO (Vinnichenko et al., 1980; Strunin, 1997; Strunin et al., 2001).

2.2. Air humidity measurements

Air humidity was measured from board the aircraft using the ultraviolet and condensation hygrometers.

The *condensation hygrometer* (ACH), designed at CAO, measures atmospheric humidity in terms of dew- or frost point. Dew/frost point is determined by measuring the temperature of a mirror cooled to a level at which dew or frost appears on its surface. The appearance of condensate is registered by an optical detector, which can distinguish between liquid and solid phases. This is very important, for the uncertainty of condensate phase on the mirror would result in considerable errors (about 2° at air temperature of −20 °C). A constant condensate amount on the mirror is maintained through feedback between the optical detector and the thermoelectric cooler power supply. A dew point (frost point) range for the ACH [3] is from +30 to −60 °C; the mirror is cooled at a 3 °C/s rate; the bias measurement error is 0.5 °C. The thermometer measuring the mirror temperature was recalibrated with the help of a working primary standard (an iron–rhodium resistance thermometer). The departure of the calibration made in 2002 from the previous one made in 1995 was within 0.3 °C. Direct comparisons in a dynamic generator of moist air "Iney," in the range from 20 to −40 °C, indicated a discrepancy within 0.5 °C.

The *Ultraviolet hygrometer* (UVH), designed at CAO, performs fast-response measurements of absolute air humidity variations. Its operation principle is based on absorption by water vapor of vacuum ultraviolet radiation at wavelengths close to the line $L-\alpha$ (121.6 nm) along the path between the radiation source and the receiver. The low noise of both the source and the receiver results in a random error of not more than 0.01 g/m^3. The response time of the instrument is 0.1 s. In different projects, this instrument was used to measure fluctuations of absolute air humidity in order to determine turbulent water vapor fluxes (Mezrin, 1997).

The instruments UVH and ACH are assembled in the same fairing ventilated in a natural way due to pressure difference along the fairing surface (see Fig. 1). The air inlet is in the rear of the fairing. Errors due to airflow disturbance, based on the observational data obtained on board a research aircraft IL-18 (Mezrin, 1992), did not exceed −0.2 °C under clear-sky conditions and +2.8% in clouds (which corresponds to +0.5÷+0.3 °C).

The UVH hygrometer, as less precise, though faster in operation, is calibrated using the condensation hygrometer ACH. For this purpose, the points from the ACH data (τ) are transferred to absolute humidity $\rho(\tau)$, with temperature T allowed for, and related to the UVH by linear regression. Regression coefficients are used to transfer UVH data to absolute humidity ρ.

[3] The instrument was also successfully used by the authors at much lower temperatures (Mezrin and Starokoltsev, 2001). However, the present version has somewhat lower characteristics.

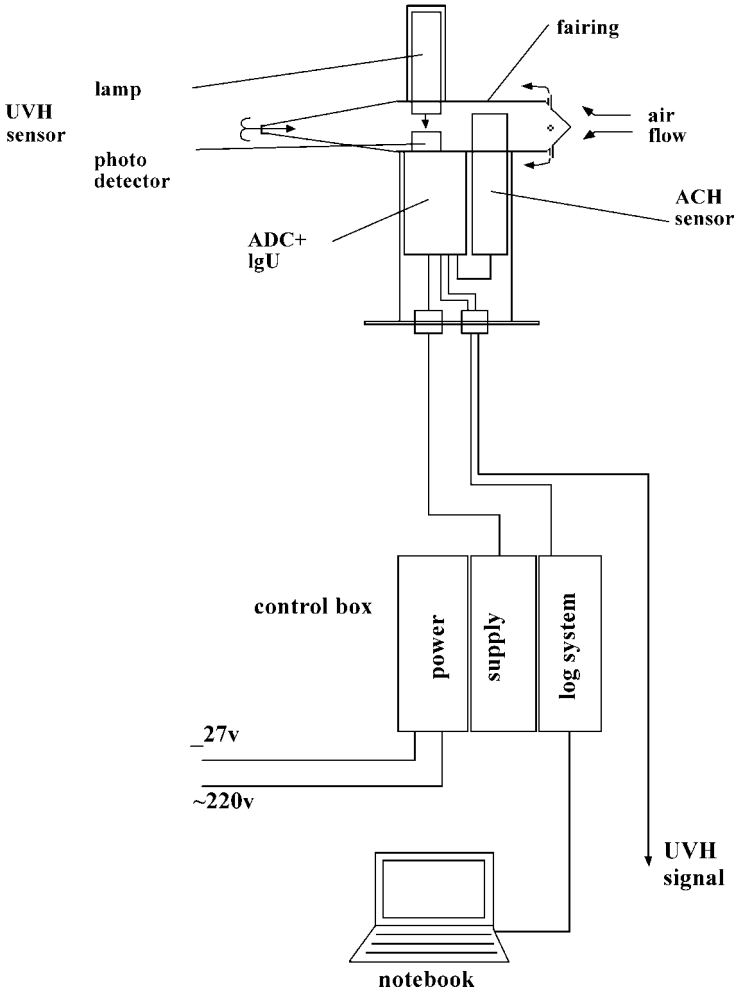

Fig. 1. Block diagram of the devices for measuring absolute air humidity and dew-point temperature.

2.3. Determining turbulent moisture flux

Vertical wind speed fluctuations, w', absolute air humidity fluctuations, ρ', and air temperature fluctuations, T', are calculated through the filtering out of the low-frequency fluctuations:

$$w' = w - \bar{w}$$

$$\rho' = \rho - \bar{\rho}$$

$$T' = T - \bar{T}$$

To calculate transport, an eddy correlation method uses the formulas:

$Q = \overline{w'\rho'}$ (g/m^{2}s) – vertical moisture transport;

$Q_l = LQ$ (W/m^2) – vertical latent heat transport,

where L is the water evaporation heat, 2500 J/g;

$Q_h = C_p \rho_a \overline{w'T'}$, W/m^2 – vertical sensible heat transport,

where C_p is the air heat capacity and ρ_a is the air density.

3. Aircraft experiment

In the course of the experiment, three flights were conducted: on 29 January, 2 February, and 3 February 2001. The last one is the most interesting to discuss.

3.1. Meteorological situation

This research flight was carried out in the cold rear of a cyclone (Fig. 2). The pressure in the cyclone center was 990.3 mbar. The cyclone shifted northeastward. The temperature was about −5 °C in the vicinity of Japan's coastline and about −25 °C along Russia's Primorye seacoast. The surface wind was about 10 m/s.

Just above the sea, cold air from the continent and warm surface water interacted. Over the sea, cumulus and cumulonimbus clouds were observed. The cold front in the eastern part of the Sea of Japan caused snow showers along the coast of Japan.

With the Siberian anticyclone restoring its influence over the coastal part of the continent, temperatures in the ground layer went down to −30 °C.

3.2. Flight description

The flight was made from Vladivostok, Russia, in the direction of Sado Island, Japan, over the Sea of Japan. The flight trajectory is shown in Fig. 3. At a 10-km distance from the coast, vertical sounding was made from a 3000-m level to as low as 100 m (Fig. 4).

Thereafter, the aircraft fulfilled four horizontal passages at altitudes of 100, 500, 1500, and 3000 m. Each of the passages lay between a sounding point and a maximum distance point.

The flight period: from 01:12 GMT (take-off) to 06:20 GMT (landing).

The wind at 1500–1000 m was 310–325°, ~ 20 m/s.

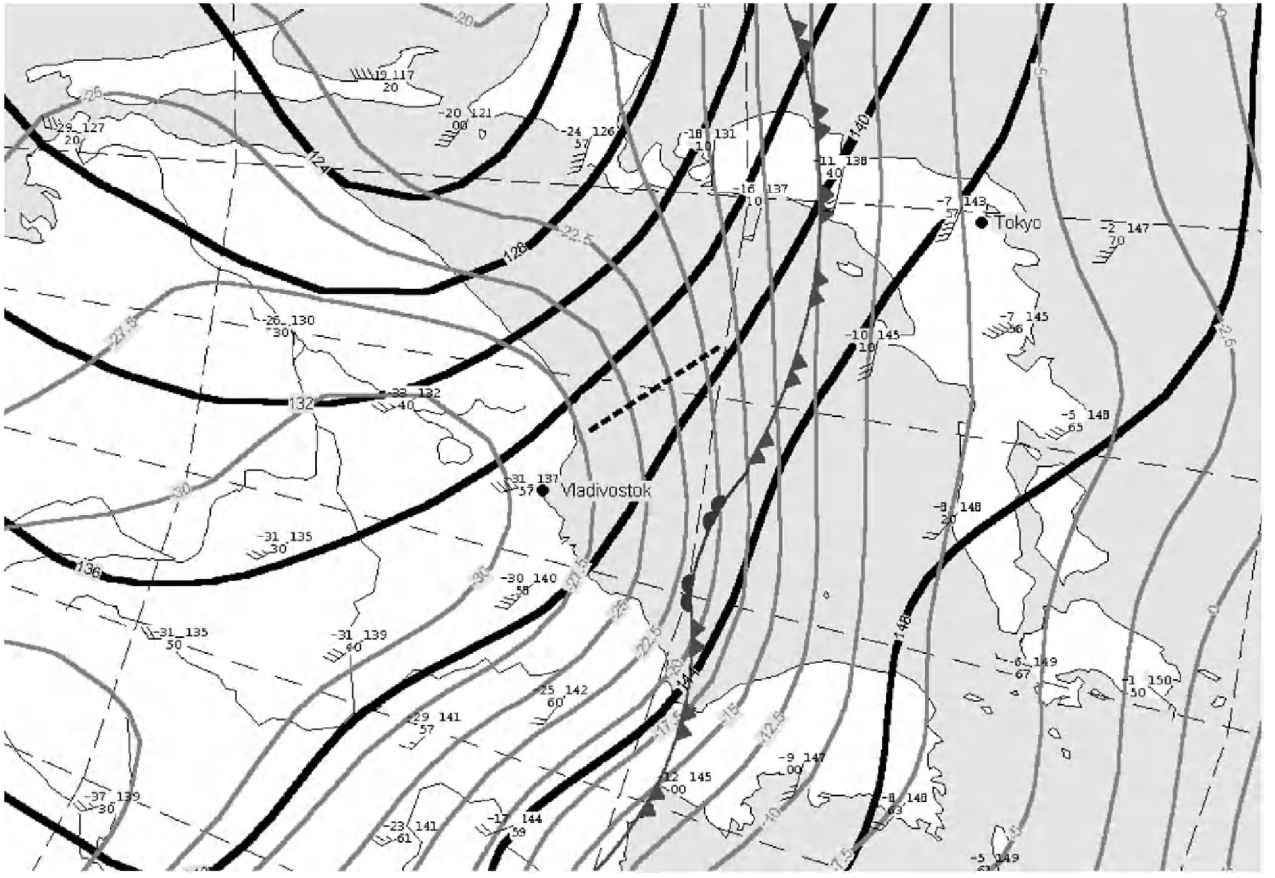

Fig. 2. AT-850, 00 GMT, 3 February 2001, Sea of Japan. The dashed line shows the direction of flight.

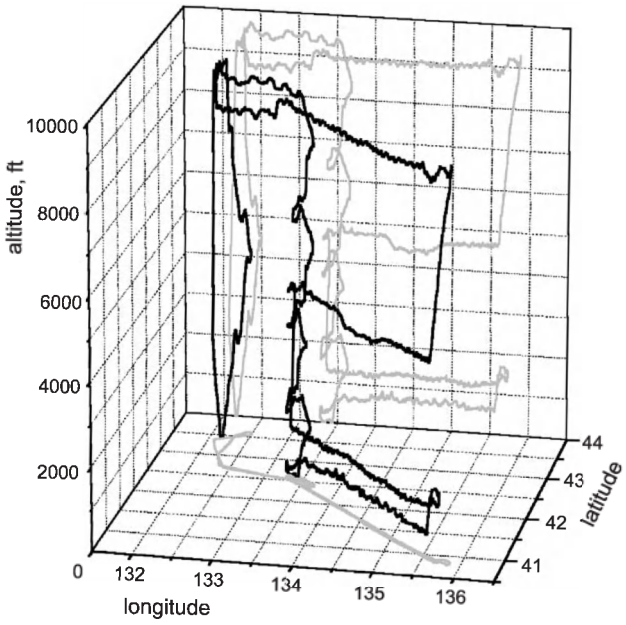

Fig. 3. 3D flight scheme, 3 February 2001.

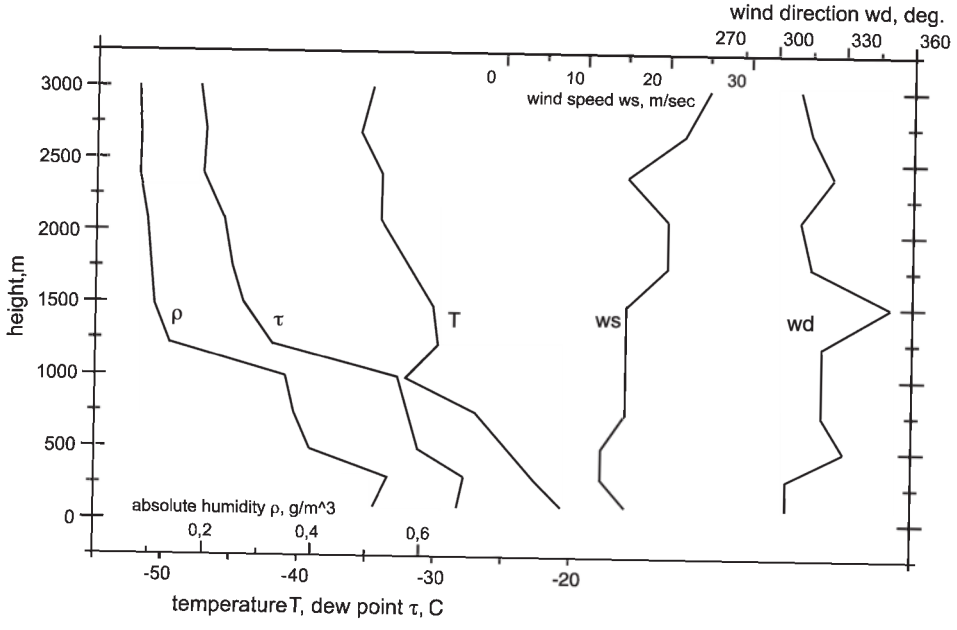

Fig. 4. Vertical sounding from a 3000-m level to 100 m: temperature, dew point, absolute humidity, wind speed, wind direction.

The flight direction was 145°, i.e., nearly parallel to the wind.

Above the water surface (at a100-m level), the temperature was −20 °C with a −27 °C frost point. At times, fog could be seen over the water. Severe turbulence was observed. Acceleration measured up to 0.37 g.

The larger the distance from the sounding point, the thicker were the clouds, from Cu hum (10% amount), with the base at 1000 m and the top at 1100 m, to Sc (100% amount), with towering clouds up to 1500 m and still higher.

4. Data analysis

4.1. Spatial variability of moisture transport

Vertical moisture transport was determined by the technique described in Sections 2.1 and 2.3. The oscillations w' and ρ' were derived from w and ρ by subtracting a 100-s sliding mean.[4] The obtained quantity $Q = \overline{w'\rho'}$ was averaged by the same sliding mean.

The value of moisture transport was estimated for all the horizontal flight sections and correlated with longitude in order to be located in space (Fig. 5).

The curve obtained for a 100-m level exhibits a spatial pattern of moisture transport with a period of about 25 km. It should be pointed out that at a 500-m level, 25-km scale features also occur, their shape and amplitude corresponding to the features observed at 100 m. The time of observing the features at those heights being different, the spatial location of the features gradually changed with time. The motion of the features is indicated by arrows. At 1.5 km, the magnitude of the moisture transport differs from zero only in the zone where the aircraft crosses cloud tops, its sign being either positive or negative. The cloud tops here seem to reach beyond the boundary layer. At 3000 m, the moisture transport is negligible.

The reason for this phenomenon becomes clear after analyzing the satellite photograph kindly submitted by the Japanese team (Fig. 6). The aircraft crosses, at an acute angle, the horizontal zones of roll circulation,[5] which causes the formation of cloud streets above 1000 m. (Horizontal flight sections are shown with a white line.) The zones of convection shift with time, which is reflected in the position of the features in Fig. 5, causing the cloud streets' shift. The distance between the cloud streets increases with the distance from the coast to reach about 10 km in the zone of observations. The convective cloud size is hardly much less, being about 7 km. Therefore, it would be hard to detect organized phenomena in passing the cloud streets across, i.e., normal to the wind

[4] This implies that we take into consideration fluctuations of less than 100 s. It will be shown below that this range is enough to determine the total transport.

[5] Horizontal roll vortices, organized roll vortices (LeMone, 1973; Chou and Ferguson, 1991; Mourad and Walter, 1996; Foster and Levy, 1998).

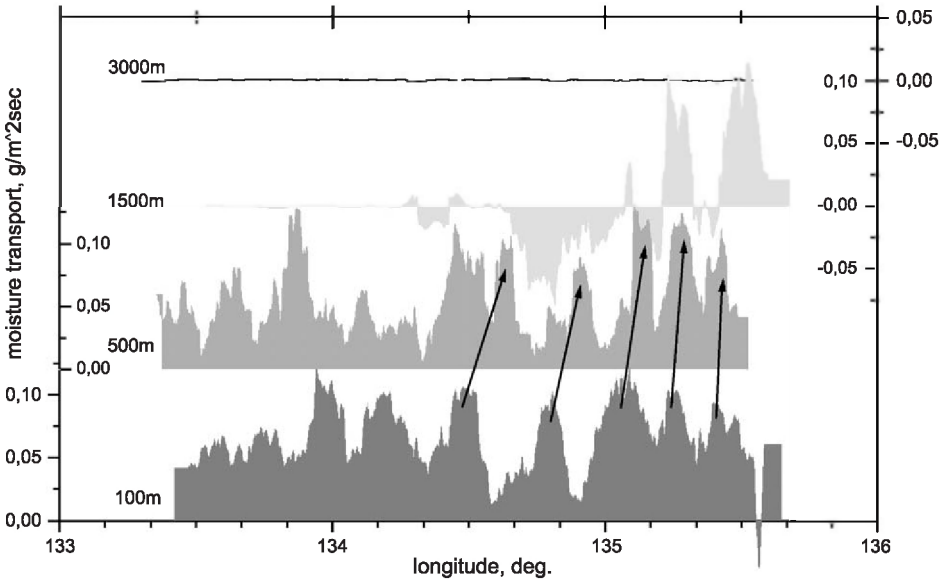

Fig. 5. Spatial features of water vapor transport at 100, 500, 1500 and 3000 m.

Fig. 6. Satellite image of clouds in the zone of the experiment.

direction. In our case, the cloud street scale—25 km—differs considerably from that of a convective cloud.

4.2. Spectral analysis of moisture transport

By using the technique described in Section 2.1, the range of the scales taken into account in calculating moisture transport can be altered. For this purpose, in calculating the flux (Section 2.3), the oscillations should be filtered with a time constant other than the 100 s previously employed. With the time constant changing from 1 to 500 s, the calculated mean (over a horizontal path) transport Q increases from 0.0025 to 0.07 g/m^2 s. The contribution of each of the scales L to the integral mean moisture transport $\Delta Q/\Delta lgL$ can be estimated. Fig. 7 presents similar results obtained by Fourier analysis.[6] The black lines refer to the measurements at 100 m, the lines shown as the contours of the gray area to those at 500 m. The graphs of the mean moisture transport Q indicate that increasing the scale to 100–500 s leads to no significant increase in the transport. (Therefore, in order to explore the spatial variability of the transport, it is enough, in our case, to consider a 0.1–100 s spectral range, which can be referred to as total.) The extreme point on the right of the graph corresponds to the scale equal to the size of the sampled area (32,768 points). Note that here the roll circulation has a 250-s scale corresponding to 25 km at a 100 m/s flight speed. While initiating the development of turbulence and convective cells, which correspond to smaller scales and make the main contribution to integral moisture transport, the circulation itself is not involved in the transport.

Fig. 8 presents a satellite cloud image for a similar case with higher resolution.[7] It enables the possibility to associate the scales involved in the transport with the horizontal size of the clouds formed due to this transport. Here, the pattern of the roll circulation is also shown.

Among the scales contributing to moisture transport the following ones can be distinguished (Fig. 7):

10–630*–1000 m (turbulence);
1000–1800*–3000 m (convective cells);

[6] The mean transport is determined using M.A. Parseval's equation:

$$\frac{1}{N}\sum_{t=1}^{N}\rho'(t)w'(t) = \frac{1}{2}\sum_{n=1}^{N/2}(A_\rho(nv_0)A_w(nv_0) + B_\rho(nv_0)B_w(nv_0)),$$

where $A_\rho(nv_0)$, $B_\rho(nv_0)$, $A_w(nv_0)$, $B_w(nv_0)$ are Fourier coefficients for $\rho(t)$ and $w(t)$, respectively. Here, N=32,768, the lowest frequency (v_0), in the series equals $1/N$ and corresponds to the size of the section under consideration. A constant component is absent as we are concerned with oscillations.

[7] As an example, a high-resolution satellite image available for a similar case is presented (01UTC, 13.01.2001, the Sea of Japan).

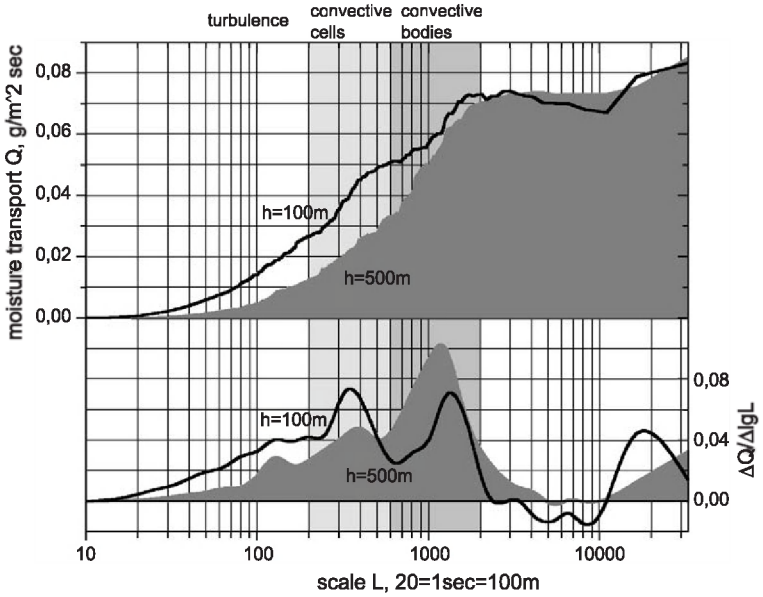

Fig. 7. Estimated moisture transport, Q, versus long-wavelength limit of oscillations considered. Spectral density of transport, $\Delta Q/\Delta lgL$, filter-smoothed with constant $\Delta lgL = 0.1$.

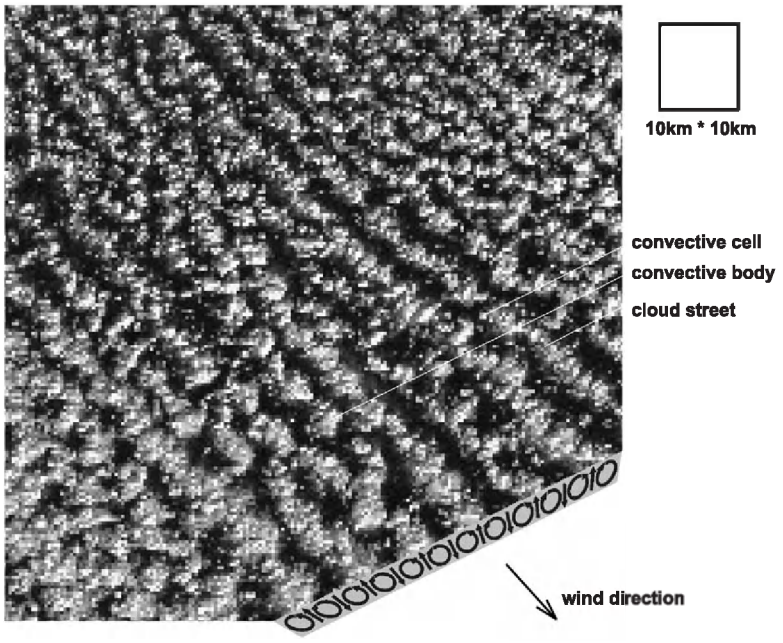

Fig. 8. A higher-resolution satellite image of clouds for a similar case (01UTC, 13 January 2001, Sea of Japan). Types and horizontal dimensions of clouds. Vertical section of assumed roll circulation.

3–6.3*–10 km (seems to be the size of a cloud, which forms after cloud street disintegration into more compact, convective mesoscale formations—convective bodies).

The values marked by asterisks (*), correspond to maximum spectral density of the transport.

At a 100-m level, each of the scales accounts for one third of the contribution to the overall transport. At 500 m, the input of small-scale decreases, while that of larger scales increases. However, the value of the mean integral transport changes far less. The share of turbulent transport in it is 1/3 and 1/6 at 100 and 500 m, respectively.

Scale	10–1000 m	1000–3000 m	3000–10000 m	Total
Moisture transport at 100 m, g/m^{2}s	0.027	0.024	0.022	0.073
(share in mean integral transport in %)	(37%)	(33%)	(30%)	(100%)
Moisture transport at 500 m, g/m^2 s	0.013	0.021	0.037	0.071
(share in mean integral transport in %)	(18%)	(30%)	(52%)	(100%)

Note that the value of the mean integral transport largely depends on the choice of an area explored. It is desirable that the number of waves (features) of spatial transport contained in this area be an integer (Fig. 5), i.e., that the number of active and passive zones be equal. With the number of passive zones larger by one, the mean value of the transport will be smaller by approximately 5%. An excess of active zones by one will results in a 5% increase of that value. Besides, the mean value of the transport changes from the start to the end of a horizontal flight leg. Therefore, let us take 5 similar features for both 100- and 500-m levels (marked in the figure by arrows). The mean values of the integral transport for these altitudes are 0.078 and 0.071 g/m^2 s, respectively.

When investigating water balance in the troposphere, one should not only consider turbulent transport as it would lead to large quantitative errors. Moreover, even qualitative conclusions may prove erroneous. Thus, in this case, turbulent moisture transport decreases with altitude by a factor of two, while the integral one changes far less.

4.3. Comparison of heat and moisture transport

A comparison of heat and moisture transports (in terms of sensible and latent heat fluxes) has indicated that their ratio at a 100-m level is approximately twice that at a 500-m level (Fig. 9). At 100 m, these quantities have a much better correlation. From the graphs, one can see that the vertical transport of sensible heat decreases faster as the altitude increases.

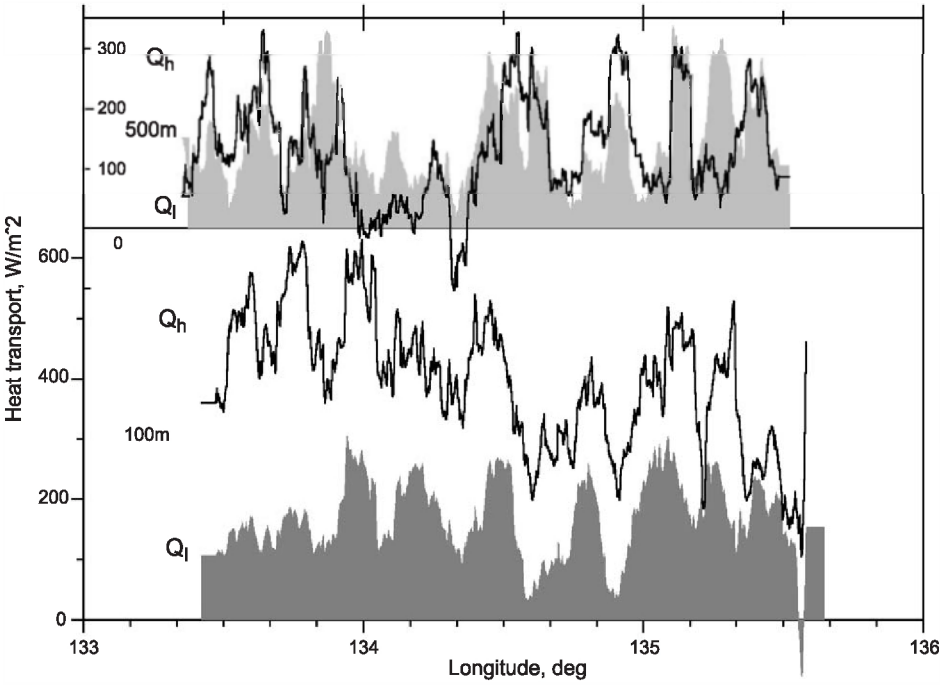

Fig. 9. Comparison of a latent (Q_l) and a sensible (Q_h) heat transport at a 100- and 500-m level.

In fact, horizontal advection carries away 161 W/m^2 of sensible heat and 25 W/m^2 of latent heat (or 0.01 g/m^2 s of moisture). The estimates[8] were obtained for a 12 m/s wind speed in a layer between 100 and 500 m, a horizontal temperature gradient of 7 °C per 250 km, and a horizontal absolute humidity gradient of 0.5 g/m^3 per 250 km.[9] The effect of mean diurnal temperature decrease (6 °C per day) and absolute humidity decrease (0.4 g/m^3 per day) is far less: it returns 33 W/m^2 of sensible and 5 W/m^2 of

[8] The calculations use the equations of moisture and heat transport (Matveyev, 1965):

$$\frac{\partial\bar{\rho}}{\partial t}+\frac{\partial\bar{u}\bar{\rho}}{\partial x}+\frac{\partial\bar{v}\bar{\rho}}{\partial y}+\frac{\partial\bar{w}\bar{\rho}}{\partial z}=-\left(\frac{\partial\overline{u'\rho'}}{\partial x}+\frac{\partial\overline{v'\rho'}}{\partial y}+\frac{\partial\overline{w'\rho'}}{\partial z}\right),$$

from which we get $\left(\frac{\partial\bar{\rho}}{\partial t}+\bar{u}\frac{\partial\bar{\rho}}{\partial x}\right)\Delta z=-\Delta Q$;

x, y, z, t are the coordinates and time (the direction of x coincides with the flight and wind direction); u, v, w are the corresponding components of wind speed;

$$\frac{\partial\bar{\vartheta}}{\partial t}+\frac{\partial\bar{u}\bar{\vartheta}}{\partial x}+\frac{\partial\bar{v}\bar{\vartheta}}{\partial y}+\frac{\partial\bar{w}\bar{\vartheta}}{\partial z}=-\left(\frac{\partial\overline{u'\vartheta'}}{\partial x}+\frac{\partial\overline{v'\vartheta'}}{\partial y}+\frac{\partial\overline{w'\vartheta'}}{\partial z}\right),$$

from which we get $C_p\rho_a\left(\frac{\partial\bar{T}}{\partial t}+\bar{u}\frac{\partial\bar{T}}{\partial x}\right)\Delta z=-\Delta Q_h$;

ϑ is the potential temperature (K).

[9] The data employed were obtained from aircraft measurements.

latent heat (or 0.002 g/m^2 s of moisture).[10] So, as the altitude changes from 100 to 500 m, one should expect a 128 W/m^2 decrease in sensible heat transport and a 20 W/m^2 decrease in latent heat transport (or a 0.008 g/m^2 s decrease in the integral moisture transport). This corresponds to the comparison results in Fig. 9 and the estimates of the integral moisture transport.

5. Conclusions

In the course of the experiment, an inflow of cold dry air from the continent (Siberia) was observed. It is this meteorological situation that is of special interest as it largely influences the weather of Japan.

As the air mass moved towards Japan, it got warmer and more humidified due to heat and moisture exchange with the open surface of the Sea of Japan. The cloud streets formed testify to the presence of a roll circulation (horizontal roll vortices).

The mean integral moisture transport has proved to be about 0.07 g/m^2 s. Upgrading the procedure of calculating vertical moisture transport has made it possible to determine this quantity within a scale range from 10 m to 50 km (0.1–500 s). Spectral analysis has revealed three scale ranges by their input to the total transport: 10–1000 m (turbulence), 1000–3000 m (convective cell), 3–10 km (convective body). Larger scales (including roll circulation scale) are not observed to make any considerable input. In this sense, the value of the transport can be considered as total. At 100 m, the inputs of the three scales are the same, while at 500 m, the role of the largest one becomes more important. However, the value of the total transport changes far less, and the share of turbulent transport in it corresponds to 1/3 and 1/6 at 100 and 500 m, respectively. When investigating water balance in the troposphere one should take it into account.

In the space structure of moisture transport obtained for the altitudes of 100 and 500 m, 25-km features were detected, which were associated with the position of cloud streets that had formed at an altitudes of 1000–1500 m. These features can be accounted for by roll circulation, which initiates the transport and cloud development. A comparison of heat and moisture transports (in terms of sensible and latent heat fluxes) has indicated that their ratio at a 100-m altitude is close to 2 and at 500 m to 1. The difference between the values of transport at the two altitudes agrees with the estimates of horizontal heat and moisture advection.

Above the boundary layer (with the upper bound at about 1500 m), the value of moisture transport is negligible.

Acknowledgements

The authors are thankful to the Core Research for Evolutional Science and Technology (CREST) of Japan Science and Technology Corporation (JST) for the financial support of this study.

[10] The sounding data shown in Fig. 4 and similar data for the previous flight of 2 February 2001 were used.

The flights conducted under severe conditions were only possible thanks to the courageous Russian pilots from the V.P. Chkalov Main Flight Test Center.

The data were collected by the research flight team, who gamely met the risks of this venture, together with the crew.

The weather analysis was prepared by Natalya Bezrukova, a meteorological scientist of the Central Aerological Observatory.

The above presentation has been made available to English-speaking readers thanks to our translator M. Khanchina and the editors of "Atmospheric Research."

References

Chou, S.H., Ferguson, M.P., 1991. Heat fluxes and roll circulation over the western Gulf Stream during an intense cold-air outbreak. Boundary - Layer Meteorol. 65, 215–248.

Foster, R.C., Levy, G., 1998. The contribution of organized roll vortices to the surface wind vector in baroclinic conditions. J. Atmos. Sci. 55, 1466–1472.

Fujiyoshi, Y., Yoshimoto, N., Takeda, T., 1998. A dual-Doppler radar study of longitudinal-mode snowbands: Part I. A three-dimensional kinematic structure of meso-γ-scale convective cloud systems within a longitudinal-mode snowband. Mon. Weather Rev. 126, 72–91.

Kato, K., Asai, T., 1983. Seasonal variations to the north and south of the polar front in the Japan Sea area. J. Meteorol. Soc. Jpn. 61, 222–238.

LeMone, M.A., 1973. The structure and dynamics of horizontal roll vortices in the planetary boundary layer. J. Atmos. Sci. 30, 1077–1091.

Matveyev, L.T., 1965. The basics of general meteorology. Atmospheric Physics. Gidrometeoizdat, Leningrad, 876 (In Russian).

Mezrin, M.Yu., 1992. Analysis of the airborne disturbances of humidity. Proceedings, CAO, vol. 180. Hydrometizdat, Moscow, pp. 129–137 (in Russian).

Mezrin, M.Yu., 1997. Humidity measurements from aircraft. J. Atmos. Res. 44, 53–59.

Mezrin, M.Yu., Starokoltsev, E.V., 2001. Aircraft condensation hygrometer and some results of measuring humidity in the zone of the equatorial tropopause. J. Atmos. Res. 59–60, 331–341.

Mourad, P.D., Walter, B.A., 1996. SAR streaks vs. cloud streets: viewing a cold air outbreak using satellite-based SAR and AVHRR imagery. J. Geophys. Res. 101, 16391–16400.

Murakami, M., Clark, T.L., Hall, W.D., 1994. Numerical simulations of convective snow clouds over the Sea of Japan: two-dimensional simulations of mixed layer development and convective snow cloud formation. J. Meteorol. Soc. Jpn. 72, 43–62.

Strunin, M.A., 1997. Meteorological potential for contamination of arctic troposphere: aircraft measuring system for atmospheric turbulence and methods for calculation it characteristics. Archive and database of atmospheric turbulence. J. Atmos. Res. 44, 17–35.

Strunin, M.A., Hiyama, T., Asanuma, J., 2001. Development of the thermal internal boundary layer and spectral characteristics of turbulence in convective boundary layer over non-homogeneous terrain. Proceedings the Fifth International Study Conference on GEWEX in Asia and GAME, Aichi Trade Center, Nagoya, Japan, 3–5 Oct., vol. 3, pp. 709–714.

Vinnichenko, N.K., Pinus, N.Z., Shmeter, S.M., Shur, G.N., 1980. Turbulence in the Free Atmosphere. Consultants Bureau, New York, 310. A division of Plenum, 227 West 17th Street, New York, NY 10011.

Yoshimoto, N., Fujiyoshi, Y., Takeda, T., 2000. A dual-Doppler radar study of longitudinal-mode snowbands: Part II. Influence of the kinematics of a longitudinal-mode snowband on the development of an adjacent snowband. J. Meteorol. Soc. Jpn. 78, 381–403.